

Photonic Integration in Indium-Phosphide Membranes on Silicon (IMOS)

Jos van der Tol^a, Rui Zhang^a, Josselin Pello^a, Frédéric Bordas^{a1}, Gunther Roelkens^{a,c}, Huub Ambrosius^a,
Peter Thijs^b, Fouad Karouta^{a2} and Meint Smit^a

^a COBRA Research Institute, Eindhoven University of Technology (TUE),
PT.12.34/35, PO Box 513, 5600 MB Eindhoven, The Netherlands

^b Philips Research Eindhoven, High Tech Campus, 5656 AE Eindhoven, The Netherlands

^c Photonics Research Group, Ghent University/imec, Sint-Pietersnieuwstraat 41, B-9000 Ghent, Belgium

J.J.G.M.v.d.Tol@tue.nl

Abstract: A new photonic integration technique is presented, which enables the use of indium phosphide based membranes on top of silicon chips. This can provide the electronic chips (CMOS) with an added optical layer (IMOS) for resolving the communication bottleneck. Very small passive devices have been realized, with performances comparable to other membrane devices (propagation loss 7 dB/cm, negligible bending loss for micron size radii, 3 dB splitter with 0.6 dB excess loss, resonator with Q-factor of 15.500). Also a new passive device is introduced, a 4.12 micron long polarization converter which in simulations promises broadband performance and tolerant fabrication. Finally, an active/passive regrowth technique is investigated for submicron active regions within an otherwise mostly passive membrane. A good morphology is obtained around the interfaces between the active and passive regions. The processing involved did not damage the materials severely, so that light emission in micro-PL measurements was found. However, an increasing blue shift with decreasing size occurred, due to quantum well intermixing. Optimizing the design and the

¹ Present address: LPN-CNRS, Site Alcatel de Marcoussis, Route de Nozay, 91460 Marcoussis, France

² Present address: Research School of Physics & Engineering, Building 60, Australian National University, ACT 0200, Canberra, Australia

processing can take care of this. Taken together, the results presented here show that it is feasible to realize extremely small passive and active devices in a photonic circuit in an InP membrane.

1. Introduction

Future microprocessors will operate with unprecedented high bit-rates that electrical interconnect networks alone cannot support. To solve this problem, it is predicted that a photonic membrane on top of the Complementary Metal Oxide Semiconductor (CMOS) circuit can provide the high-speed on-chip data transport needed to give new life to the computing industry [1]. Conversely, building blocks for future optical data communication need to be scaled down together with the electronics driving them in order to lower fabrication costs, power consumption and footprint. Therefore, it is clear that electronics and photonics can both greatly benefit from being integrated on the same chip.

In order to create a photonic interconnect layer on top of electronic chips, different materials and processes can be considered. Because of its relative degree of compatibility with the mature CMOS technology, Silicon-on-insulator (SOI) is considered a suitable material [2]. Many high-quality photonic components, including high-speed modulators and photodetectors [3], have already been demonstrated using SiGe technology. However, due to the indirect bandgap of silicon, SOI alone cannot easily integrate the optical sources and amplifiers necessary for generating and maintaining the optical signals in a photonic interconnect network. This problem has been addressed in different ways [4-10], four of which are presented in Fig.1.

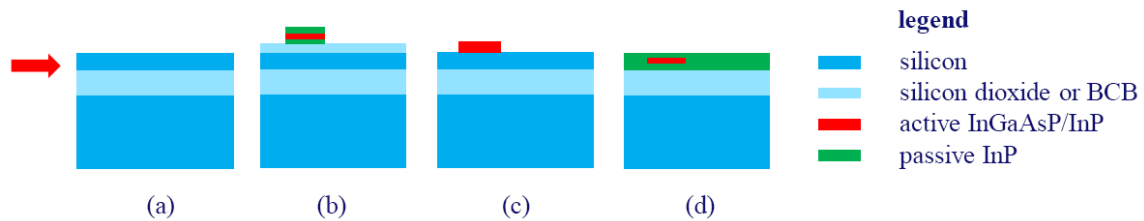


Figure 1: Schematics of four different ways to generate light in a photonic layer on top of a silicon IC

In [8,9] an approach is followed where light is coupled from an external (off-chip) source into the passive SOI circuit (see Fig.1a). This approach is technologically less challenging than other methods and,

therefore, the best candidate for early applications. However, due to the lack of on chip light generation and amplification the scalability of this approach to higher circuit complexities is limited. In [10] another approach is followed, depicted in Fig. 1b, which relies on the evanescent coupling of light from a laser source processed in a III-V layer stack on top of the passive silicon circuit via a silicon waveguide to a III-V detector on top of the silicon circuit. However, the coupling efficiency of the optical tunnelling through the low-refractive-index layer between the laser and the SOI waveguides is becoming increasingly more difficult to control if the lasers get smaller. A slightly different method, proposed by Fang et al. [5], proposes to bond and process an active InGaAsP/InP layer on top of the silicon layer which provides gain to the silicon waveguides (see Fig. 1c). Also in this elegant method, finding a good compromise between low-coupling loss and high gain is difficult.

In the present paper, we describe a new approach: An Indium-phosphide Membrane on Silicon (IMOS) which proposes to replace the silicon membrane with an InP-membrane that contains both passive and active regions (see Fig. 1d). This brings a number of advantages in comparison to the other mentioned methods. First, as light is kept in a single optical layer the coupling between active and passive components is greatly alleviated. This coupling does not depend anymore on an intermediate layer and alignment problems with respect to the underlying silicon circuit are reduced. Also, there is a large flexibility with respect to the silicon carrier; due to the use of thick polymeric bonding layers (benzocyclobutene , BCB) any surface morphology can be used there. We demonstrate in the following that an InP-membrane allows for passive optical devices with fully acceptable performance, and how small active components can be integrated with these devices by submicron size selective area growth.

2. Realized passive IMOS components

In this section a description is given of the fabrication and the results of a number of IMOS passive devices [6, 7]. These include gratings for coupling light into and out of the membrane, photonic wires, bended waveguides, MMI-couplers and ring resonators.

2.1. Fabrication

The fabrication of IMOS devices starts from a layer structure containing a 200 nm InP-membrane layer on top of 3 etch-stop layers (InGaAs-InP-InGaAs) on an InP-substrate (Fig. 2.1). In this layer stack a pattern is defined by e-beam lithography with a positive resist on a 50 nm thick SiN_x layer, deposited by PECVD. After development and post-bake of the resist, the layer is etched with a CHF₃-based RIE to transfer the pattern into a hard mask. The resist post-bake reduces the sidewall roughness, which is critical for low propagation losses in the photonic wires. Optical lithography is used to cover the area where gratings will be made (see section 2.2). A CH₄/H₂ based ICP etching step follows, to etch the open part through the whole InP membrane. After removal of the resist, a second etch step of 70 nm is performed for the gratings. Finally the SiN_x hard mask is removed with a HF solution.

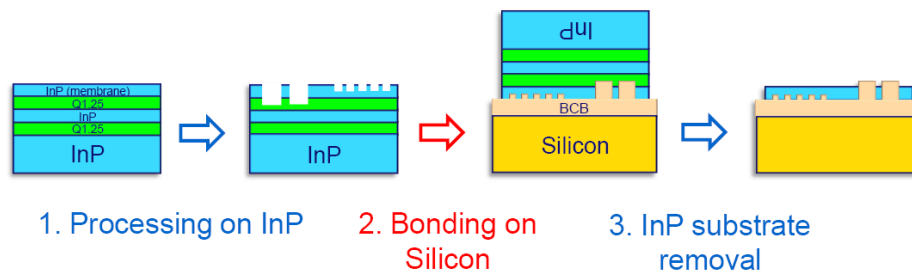


Figure 2: IMOS fabrication scheme

After pattern definition, a BCB layer of 780 nm is spin-coated onto the InP-sample, and cured for 1 hour at 250°C in a nitrogen environment. Then, the sample is bonded onto a host-substrate with a 1 μm thick BCB-layer [11] (Fig. 2.2). This BCB-layer is also cured for 1 hour at 250°C in a nitrogen environment. The InP-substrate is removed using lapping and wet-etching in HCl until the InGaAs etch stop layer is reached. Finally, the InGaAs-InP-InGaAs etch-stop layer stack is removed using three selective wet etching steps (Fig.2.3).

2.2. Grating couplers

The gratings are designed for an optimal coupling with a wavelength of 1.55 μm at an angle of 10°. The depth of the gratings is 70 nm, to allow for an efficient overlap of the diffracted field with an optical fiber mode (mode field diameter of 10.4 μm). The grating period is 730 nm, with a filling factor of around 50%.

The optimal simulated BCB thickness is $780 \text{ nm} + p \cdot \lambda / 2n$, where λ is the wavelength in vacuum, p an integer, and n is the refractive index of the BCB layer. In our case $p=1$. This particular thickness allows for maximum diffraction efficiency towards the air superstrate, which maximizes the fibre-chip coupling.

Transmission measurements are performed with a tuneable laser as a source. The grating area is $10 \times 10 \mu\text{m}^2$, and the device consists of a $50 \mu\text{m}$ long 400 nm wide wire and $600 \mu\text{m}$ long tapers on each side. The measured fibre-to-fibre loss at the peak wavelength is 6.8 dB . As the wire is very short, we assume that

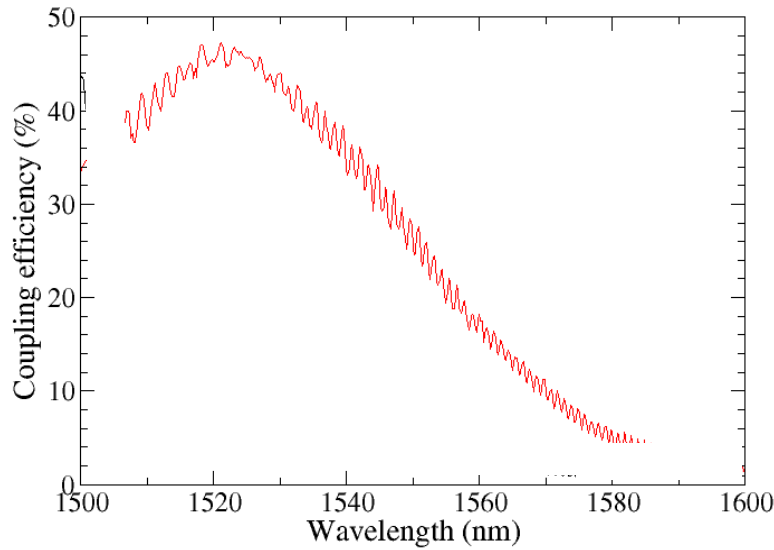


Fig. 3: Coupling efficiency for the grating coupler.

losses primarily arise from the two grating couplers. This assumption will be confirmed in paragraph 2.3.

Figure 3 shows the coupling efficiency of the grating. The maximum coupling efficiency is 47%.

2.3. Wires

Photonic wires of four different lengths and 400 nm width are fabricated in order to determine the losses.

Fig. 4(left) shows the transmission through $500 \mu\text{m}$, $300 \mu\text{m}$, $100 \mu\text{m}$ and $50 \mu\text{m}$ length of wire connected to two grating couplers. No differences in transmission can be seen for the different lengths. Therefore an upper boundary of 10 dB/cm for the propagation losses can be deduced. This confirms the assumption made in the preceding paragraph that the propagation loss of a $50 \mu\text{m}$ long wire can be neglected. This quite low propagation loss value will be confirmed by the results for the ring resonator in section 2.6.

2.4. Bends

Three different 180° S-bends are realized, with radii of $40\ \mu\text{m}$, $20\ \mu\text{m}$, and $5\ \mu\text{m}$. The transmission for waveguides containing these bends is shown in Fig. 4(right). It was not possible to measure any difference between bends of different radius. This shows that very compact integrated optical circuits can be fabricated using very sharp bends.

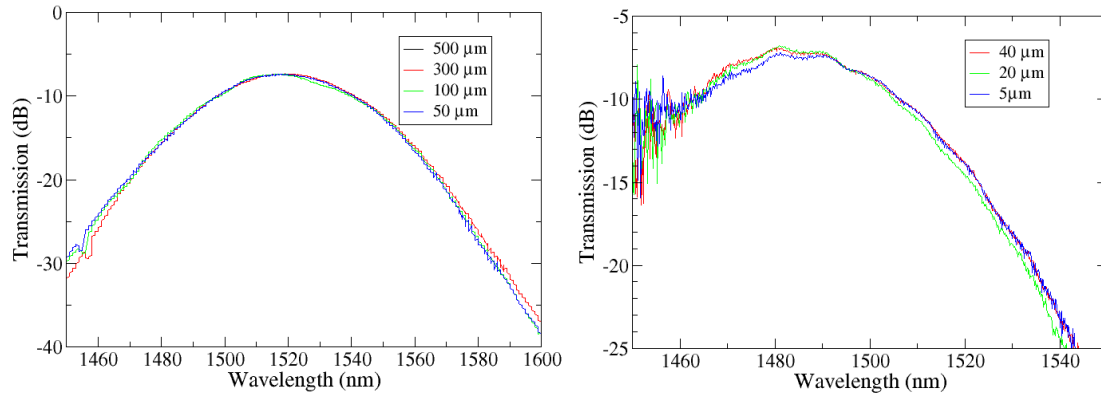


Fig. 4 Left: Transmission through 400 nm wide wires of different lengths, connected to two grating couplers.

Right: Transmission through S-bends of $40\ \mu\text{m}$, $20\ \mu\text{m}$, and $5\ \mu\text{m}$, connected to two grating couplers.

2.5. MMI's

The fabricated MMI's are 1×2 couplers. Fig. 5(left) shows a SEM image of the device. The dimensions of the MMI are $6.64 \times 2.75 \times 0.2\ \mu\text{m}^3$. Transmission measurements on the device are shown in Fig. 5(right).

The reference (upper line) is a $50\ \mu\text{m}$ long wire without MMI, connected to two grating couplers.

Transmission through the two output branches is very comparable, and 3.6 dB lower than the reference.

Hence the fabricated MMI coupler operating as a 3dB splitter shows an excess loss of 0.6 dB.

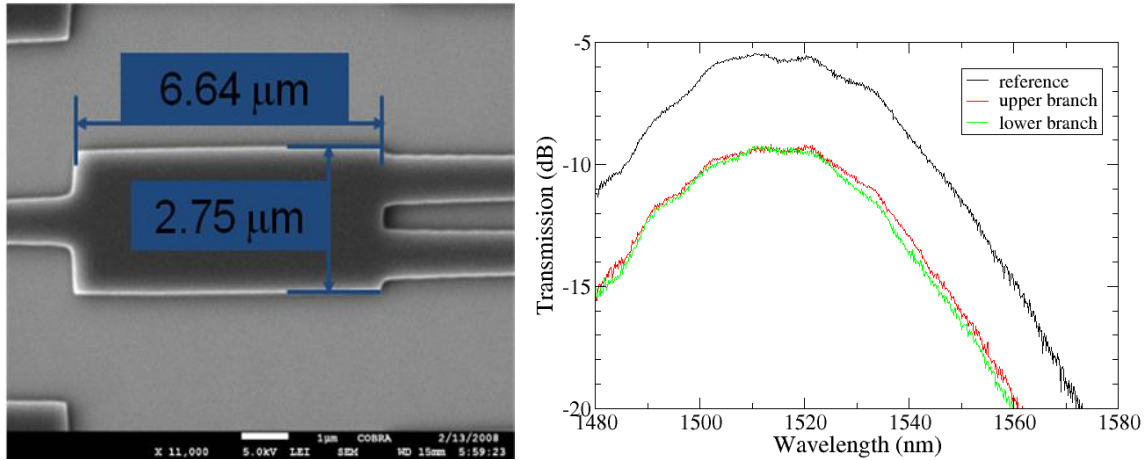


Fig.5: left – SEM image of a fabricated MMI ; right – transmission through both output branches, together with the reference, connected to two grating couplers.

2.6. Ring resonators

Two generations of ring resonator notch filters are realized. Here an improved result with respect to our earlier work [6] is reported. The device is depicted in fig. 6(left). Light is coupled to the ring from a straight wire through a directional coupler. One resonance peak is shown in fig. 6(right).

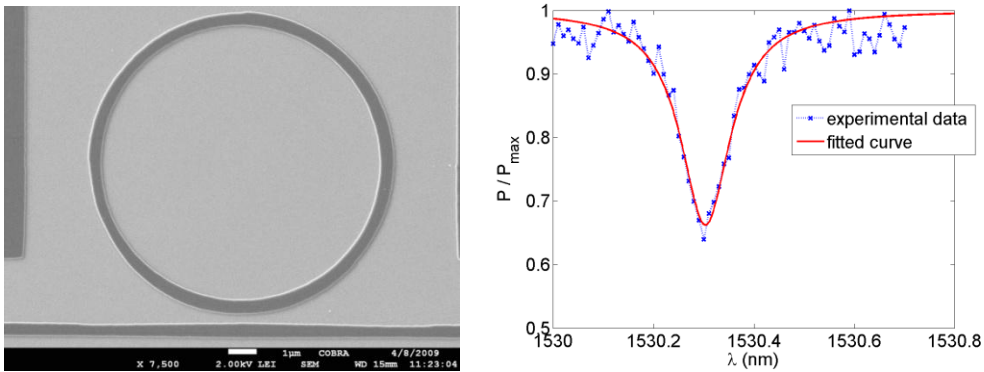


Fig. 6: Left-SEM photograph of the ring resonator with 7 μm radius. Right-transmission spectrum at the resonance peak.

From this measurement the loaded Q-factor, defined as f_0/FWHM with f_0 the central frequency and FWHM the full width at half maximum, is found to be 15500. This Q value is certainly enough to ensure lasing

action with active material and modest gain. A fit of the theoretical formula [12] to the experimental peak, centred on $\lambda = 1530\text{nm}$, showed propagation losses in the ring of about 7 dB/cm. These losses correspond to those measured on straight wires (section 2.3). We expect to further lower the loss in subsequent optimisation. The coupling constant in the directional coupler is low, $7 \cdot 10^{-3}$, because the coupling gap is relatively large, leading to undercoupling. This explains the relatively shallow dip of the resonance peak.

3. A novel passive IMOS device: polarization converter

In this section a new device, an ultra-small polarization converter (PC) in IMOS, is introduced, using two oppositely-oriented triangular waveguide sections [13]. The presented device is more than one order of magnitude smaller than the shortest polarization converters made by optical lithography on classical III-V substrates [14], and was designed with a clear fabrication plan which uses the standard technological tools available for InP processing. The polarization conversion behaviour is analyzed using the Film Mode Matching (FMM) method [15]. This component can be applied to polarization- diversity integration schemes and in interesting devices such as light intensity modulators and polarization bit interleaving (PBI) components [16].

3.1. Principle

The idea behind the use of asymmetrical cross-section waveguides in PCs is to create a new set of two eigenmodes which are not aligned with the TE and TM polarization of the normal rectangular waveguides, and which propagate with different propagation constants β_1 and β_2 . The incoming polarization state, e.g. TE in Fig. 7, is projected on these two tilted eigenmodes. As the eigenmodes propagate with different speeds, a phase-shift is created between them that linearly increases with the propagation length L (the same birefringence principle as in bulk half-wave plates). By choosing the length L of the triangular section and coupling light back to a rectangular waveguide, different elliptical and linear polarization states can be obtained at the output.

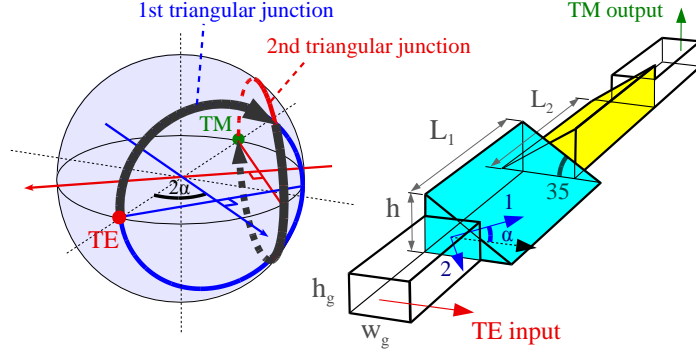


Figure 7: Schematic of the polarization converter design and Poincaré sphere diagram of the polarization conversion.

The triangular waveguides can be obtained by dry etching of the vertical wall and wet etching of the slanted wall at an angle of 35° with respect to the (001) plane [17]. The resulting asymmetry yields a rotation $\alpha \sim 23^\circ$ (determined using the FIMMWAVE mode solver [15]) of the eigenmodes of the triangular waveguides. As a consequence, the polarization states attainable by varying the length of the first triangular waveguide are all the states represented by the first drawn circle on the Poincaré sphere in Fig. 7. In order to achieve full TE to TM conversion, one triangular section is not enough. Therefore, another triangular section is added, mirrored with respect to the first one, which will enable the TM polarization state to be reached by rotating along the semi-dotted circle on the sphere in Fig. 7. The two bold arrows in the sphere show how the polarization is gradually converted from TE to TM. The respective lengths of the two triangular sections for full TE to TM conversion can be expressed in terms of the half-beat length

$L_\pi = \frac{\pi}{\beta_1 - \beta_2}$ and the tilt angle α as:

$$L_1 = \frac{L_\pi}{\pi} \times \left(\arcsin \left(\frac{1}{(\tan 2\alpha)^2} \right) + \frac{\pi}{2} \right) = 2L_\pi - L_2 \quad (1)$$

The device has a total length of $2L_\pi$.

3.2. Design optimization and tolerances

The structure is modelled in FIMMWAVE, taking into account the Benzocyclobutene (BCB) and air claddings of a fabricated device (see Sections 2.1. and 3.3.).

We first investigate the performance of the PC at a wavelength of $\lambda = 1.55 \mu\text{m}$. The propagation constants β_1 and β_2 of the two modes of the triangular waveguides are calculated for different values of the membrane height h . It is found that the highest birefringence is obtained for $h = 400 \text{ nm}$. The corresponding half-beat length is equal to $L_\pi = 2.06 \mu\text{m}$, which corresponds to a total device length of only $4.12 \mu\text{m}$. After setting h to this value, the cross-section dimensions h_g and w_g (see Fig. 7) of the input (and output) rectangular waveguides, as well as the lateral offsets between the different junctions are optimized to maximize the coupling efficiency. It is found that the coupling between rectangular and triangular waveguides is optimized for $h_g/h \sim 2/3$. This suggests the use of a very thin etch-stop layer in the membrane to enable a simple and accurate definition of these two heights. A 20 nm-thick quaternary etch-stop layer was therefore included in the simulation of the triangular waveguides.

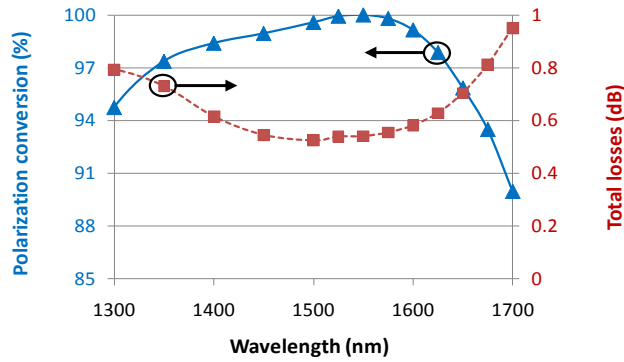


Figure 8: Spectral behaviour of the proposed PC design optimized for $\lambda = 1.55 \mu\text{m}$

The behaviour of the PC and its tolerance to different fabrication parameters variations is simulated. Fig. 8 shows that the short length of this PC makes it very broadband. For the 1.4-1.6 μm wavelength range, the device insertion loss is less than 0.6 dB and the polarization conversion (defined as the TM output power divided by the total output power for a fully TE polarized input wave) is more than 98%. Furthermore, the use of wet-etching, which enables to set the slope of the slanted wall of the triangular junctions very accurately to 35° and to define the two heights h and h_g , makes our design intrinsically tolerant. According to our simulations, an error of 20 nm in the definition of the height h of the triangular section (respectively, an error of 100 nm in the rectangular waveguides width) increases the losses by only 0.1 dB without changing the polarization conversion.

3.3. Fabrication plan

Like our previous IMOS components (Section 2)), the presented polarization converter will first be fabricated on an epitaxial InP and quaternary layer structure. Then, the sample is bonded upside-down with BCB on a host wafer and the substrate and sacrificial layers are removed. In the end, only the submicron-thick patterned InP membrane is left, embedded in BCB and its bottom surface facing the air (see Fig.2). For the triangular waveguides, we propose to adapt the process flow successfully applied in classical InP-based polarization converters [14]. First the heights h and h_g are defined using the quaternary etch-stop layer mentioned in the previous section (see Fig.9a). The rectangular waveguides can then be fabricated by standard e-beam lithography and dry-etching as in [18], together with the vertical sidewalls of the triangular waveguides (see Fig.9b). The chip is then covered with a SiN_x mask which is dry-etched on the area of the triangular sections to leave only the vertical sidewalls covered (see Fig.9c). Successive wet-etchings of InP, using e.g. $1\text{HCl}:1\text{H}_3\text{PO}_4$ [17], and of the thin quaternary etch-stop layer, will stop on the (112) plane between the SiN_x covered wall and the etch-stop layer below, thus defining quasi-perfect triangular cross-section waveguides (see Fig.9d).

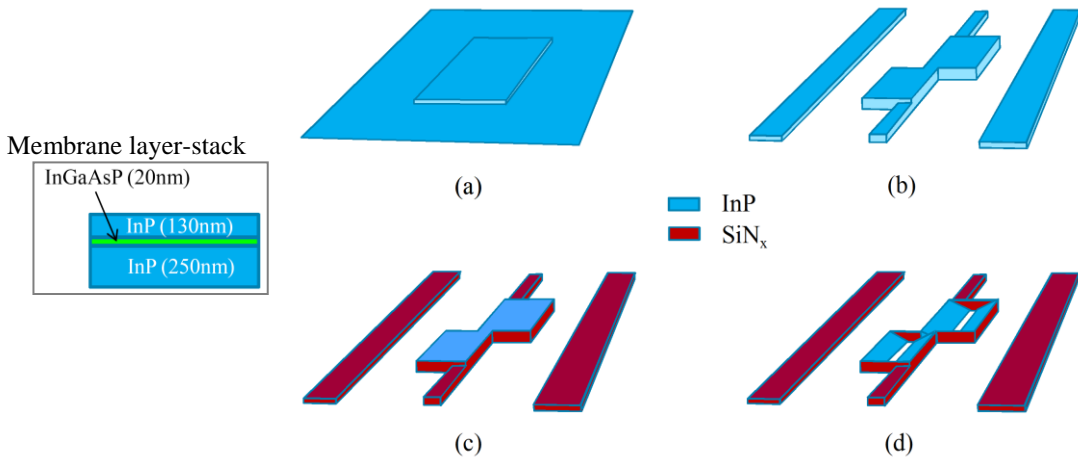


Figure 9: Fabrication process design for the PC

This device can be used with other devices of the IMOS platform to add polarisation handling and control capabilities to the IMOS technology and realize high-density and eventually fully active-passive PICs suitable for inter and intrachip communication.

4. Active-passive integration in IMOS using selective-area growth

The major advantage of InP-based membranes over e.g. Si-based membranes is the possibility to include active devices (lasers, amplifiers). Since the high index contrast in the membrane results in very small devices (as compared to traditional InP-based integration, [19]), this requires the realization of micron-size or even submicron size regions of active material in an otherwise passive membrane. Successful active-passive integration with submicron active regions in membranes is thus an essential step towards complete PICs. In this section results are presented on active-passive integration with sub-micrometer active areas [20].

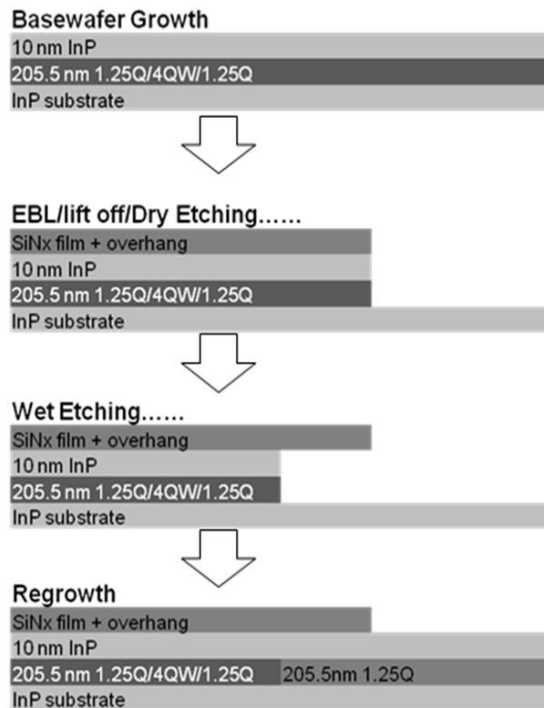


Figure 10. Fabrication process flow

The active-passive integration should satisfy two critical conditions. On one hand, a smooth and flat interface should be realized between the active and passive materials. A rough interface causes both reflection and scattering loss when light is coupled between active and passive regions. Meanwhile a good

surface flatness is required for processing and bonding of membranes. On the other hand, since the smallest active regions are around submicron size, it is possible that the active quantum well materials will be damaged by the processing. To check the quality of the active-passive integration, active regions of multiple shapes (such as hexagons and octagons) and different orientations are realized. The size of the active regions varies from about $0.25 \mu\text{m}^2$ to $25 \mu\text{m}^2$.

4. 1. Fabrication

As it is shown in Fig.10, the starting point is a 200 nm quaternary layer (InGaAsP) on InP substrate as this is a typical thickness for membranes. Quantum wells (QWs) embedded in the InGaAsP layer are designed to emit light at $1.55 \mu\text{m}$. The quaternary layer with the QWs is etched away, except for the places where an active medium is required. This is done using a combination of dry etching (CH_4/H_2) and wet etching. Then a regrowth of passive material leads to a passive quaternary layer with an embedded local active medium. The wet etching time is optimized to obtain a suitable underetch, that results in a flat surface around the interface between active and passive regions.

4.2. Characterization

The quality of the submicron active regions is determined by SEM inspection of the morphology, and by micro-photoluminescence of active regions to determine the quality of the remaining QWs materials. It was found that there are no differences between the various shapes and orientations. This indicates that the processing and the regrowth do not depend significantly on the crystal orientation of the substrate.

Interface morphology

The quality of the interface between active and passive materials is checked using Focused Ion Beam (FIB) etching and SEM inspection. Fig. 11 shows a top view SEM picture of a realized structure (hexagon) with a submicron size. The SiN_x mask is left on the sample, to make the active areas visible. The line indicates the position where the cross section picture of Fig. 12 is made, by the use of FIB etching and SEM. The good quality of the interface and the flatness of the surface can be seen in this picture.

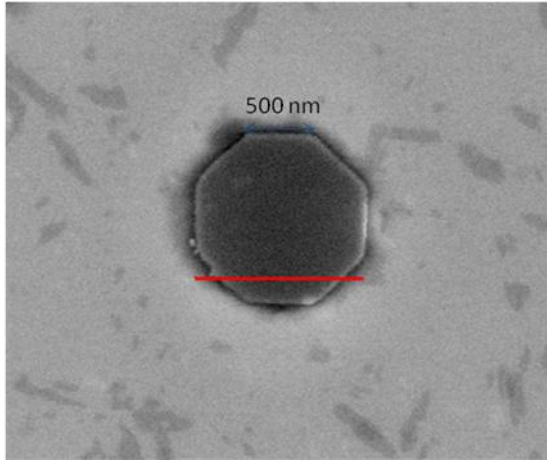


Figure 11. SEM picture (hexagon)

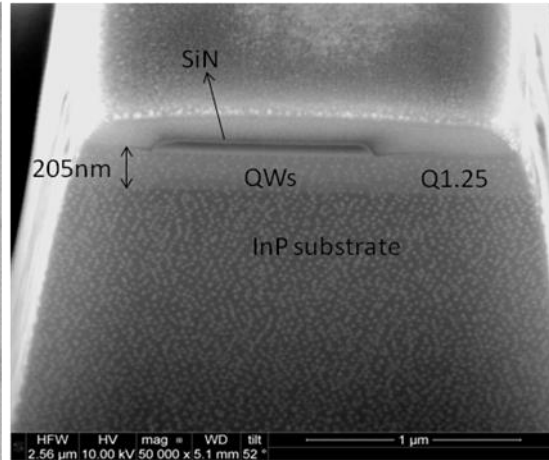


Figure 12. Cross section made by FIB

Micro-Photoluminescence (PL) measurement

Fig. 13 shows the micro-photoluminescence of a realized structure (octagons) under CW pumping by a red laser diode at 660 nm. The spectrum corresponds to the QWs emission with a peak centred on 1500nm. More analysis on micro-PL measurements are shown in Fig. 14 and Fig. 15. The relation between PL integrated intensity and active area size is shown in Fig. 14. The PL integrated intensity increases with the active area size which implies that the processing did not result in a “dead zone” of damaged (non-emitting) material at the edges of the active regions.

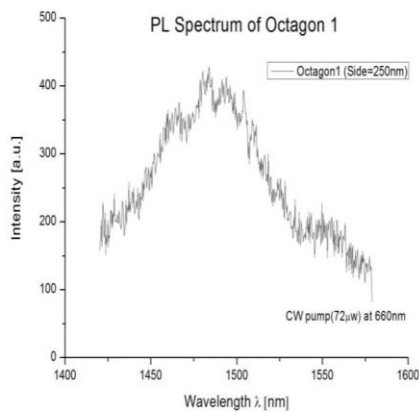


Figure 13: PL spectrum of a submicron QWs region

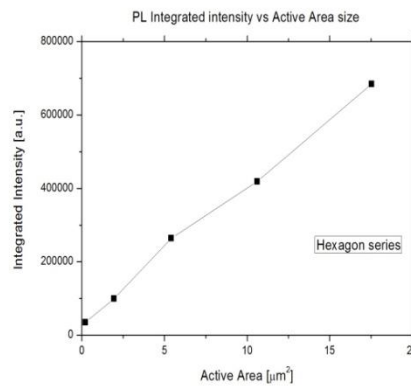


Figure 14: PL integrated intensity vs. Active area size

Fig. 15 shows how the PL integrated intensity increases with pumping power. Also here no indication of degraded material is found, which would show up as non-radiative recombination.

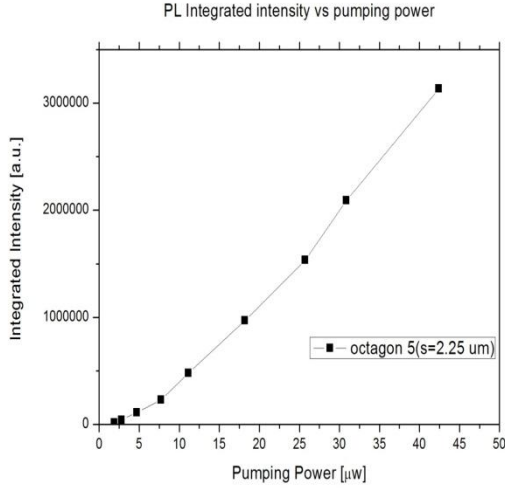


Figure. 15: PL integrated intensity vs. pumping power

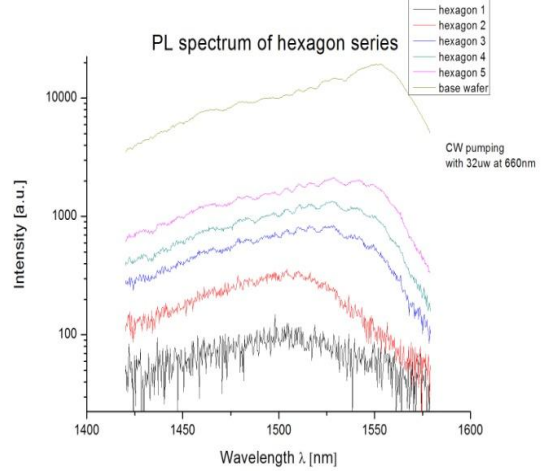


Figure. 16: PL spectrum showing the blue shift.

However, an increased blue shift is observed when the size of the active region decreases (see Fig. 16). We believe that this is due to the QW intermixing effect. QW intermixing involves the inter-diffusion of constituent atoms across the well barrier interfaces and is a well known technique to modify the band gap of QWs [21]. In our case it happens unintentionally. During the fabrication process, Reactive Ion Etching (RIE) is used to etch the structure and it is known that defects will be formed on the side walls during this fast dry etching process. In the regrowth process which is going on under very high temperature (up to 600°C). These defects will diffuse to the QWs and cause the intermixing. The smaller the structure, the easier for the defects to diffuse into the centre of the active region and thus the larger the blue shift will be. Compensation of the wavelength shift can be made during the QW design in advance. Moreover, our results show that a somewhat longer time of chemical wet etching can remove side wall defects partially and therefore reduce the blue shift.

In conclusion these results indicate that it is feasible to realize active-passive integration within the submicron scale on a quaternary material system (InGaAsP). The last important hurdle towards the realisation of very small lasers in InP-based membranes with very low threshold current and power

consumption is the development of a low-loss structure for efficient current injection into the submicron active region. This hurdle is the subject of our present research.

5 Conclusions

Photonic integration on InP-based membranes has been investigated. This technique could provide a much needed optical transport layer to silicon based electronic chips. The membrane geometry leads to very small devices and integrated circuits, while the use of InP/InGaAsP layer stacks allows both passive (waveguiding, splitting, filtering, filtering) and active (light generation and amplification, detection) functions to be realized. A fabrication technology is developed which uses BCB-bonding of a processed layer stack on silicon, followed by subsequent removal of the InP-substrate. With this technique a number of passive devices have been realized, which show acceptable performance parameters (propagation loss 7 dB/cm, negligible bending loss for micron size radii, 3 dB splitter with 0.6 dB excess loss, resonator with Q-factor of 15.500). Furthermore, a device for polarization handling in the membrane is designed and simulated: a two section polarization converter of only 4 μm length with good tolerances. Realization of this device is under way. Finally, the possibility of very small lasers in the membrane is studied by realizing submicron size active regions. For this an active passive regrowth technique is developed. The resulting structures showed a good morphology, which is important for subsequent processing, while light emission was obtained from even de smallest active areas ($0.25 \mu\text{m}^2$). An increasing blue shift with reducing size was found, probably due to QW intermixing, which can be controlled by adjusting the QW-design and the processing.

Together the results presented here indicate the feasibility of photonic integrated circuits, so including both active and passive functions, in a membrane on top of a Si-chip. However, a number of problems still needs to be addressed before the concept is fully operational. A technique has to be developed to efficiently supply currents and voltages to the active devices on the membrane. Furthermore, also the thermal management and the mechanical stability of the membranes need to be addressed. Our next research efforts will focus on these issues.

Acknowledgment: This work is supported by the European Commission in the HISTORIC project.

REFERENCES

- [1] Carloni, L. et al, " Networks-on-chip in emerging interconnect paradigms: Advantages and challenges", Proc. 2009 NOCS, San Diego (CA), May 10 - 13, 2009.
- [2] Jalali, B., and Fathpour, S.: 'Silicon Photonics', J. Lightwave Technol., 2006, 24, (12), pp. 4600-4615
- [3] Assefa, S., Xia, F.N., and Vlasov Y.A.: 'Reinventing germanium avalanche photodetector for nanophotonic on-chip optical interconnects', Nature, 2010, 464, pp. 81-84
- [4] Liu, L., Roelkens, G., Van Campenhout, J., Brouckaert, J., Van Thourhout, D., and Baets, R.: 'III-V/Silicon-on-Insulator Nanophotonic Cavities for Optical Network-on-Chip', J. Nanosci. Nanotechnol., 2010, 10, pp. 1461-1472
- [5] Fang, A.W., Park, H., Cohen, O., Jones, R., Paniccia, M.J., and Bowers, J.E.: 'Electrically pumped hybrid AlGaInAs-silicon evanescent laser', Opt. Express, 2006, 14, (20), pp. 9203-9210
- [6] Bordas, F., Roelkens, G., Zhang, R., Geluk, E.J., Karouta, F., van der Tol, J.J.G.M, van Veldhoven, P.J., Nötzel, R., van Thourhout, D., Baets, R., and Smit, M.K.: 'Compact Passive Devices in InP Membrane on Silicon', in Proc. ECOC 2009, Vienna, Austria, 20-24 September 2009, paper 4.2.4
- [7] Bordas, F., Roelkens, G., --- : "---", Opt. Express, to be published
- [8] Vlasov, Y. et al, 'High-throughput silicon nanophotonic wavelength-insensitive switch for on-chip optical networks', Nature Photonics 2, 242 - 246 (2008)
- [9] Batten, C. et al, Proc. HOTIC 2008, Stanford, CA, USA 2008, pp. 21-30.
- [10] D. Van Thourhout et al, 'A Photonic Interconnect Layer on CMOS', Proc. European Conference on Optical Communications, paper 6.3.1 (2007)
- [11] Roelkens, G., J. Brouckaert, D. Van Thourhout, R. Baets, R. Nötzel and M. Smit, "Adhesive Bonding of InP/InGaAsP Dies to Processed Silicon-On-Insulator Wafers using DVS-bis-Benzocyclobutene", J. Electrochem. Soc., vol. 153, pp. G1015-G1019, 2006.

- [12] Schwelb O. : 'Transmission, Group Delay, and Dispersion in Single-Ring Optical Resonators and Add-Drop Filters- A Tutorial Overview', J. of Lightwave Techn., Vol. 22, no. 5, pp. 1380-1394, 2004.
- [13] Pello, J. et al: 'Design of a new ultra-small polarization converter in InGaAsP/InP membrane', Proc. ECIO 2010, Cambridge (UK), paper WeB2.
- [14] Augustin, L.M., Hanfoug, R., van der Tol, J.J.G.M., de Laat, W.J.M., and Smit, M.K.: 'A compact integrated polarization splitter/converter in InGaAsP-InP', IEEE Photon. Technol. Lett., 2007, **19**, (17)
- [15] FIMMWAVE v.5.1, Photon Design, 2008
- [16] Cho, P.S., and Khurgin, J.B.: 'Return-to-zero differential binary phase-shift-keyed multichannel transmission with 25-Gbit/s polarization bit interleaving and 25-GHz spacing', Journal of optical networking, 2003, **2**, (5)
- [17] Adachi, S., and Kawaguchi, H.: 'Chemical Etching Characteristics of (001) InP', J. Electrochem. Soc., 1981, **128**, (6), p. 1342
- [18] Bordas, F., van Laere, F., Roelkens, G., Geluk, E.J., Karouta, F., van Veldhoven P.J. et al.: 'Compact grating coupled MMI on DVS-BCB bonded InP-membrane', 14th European Conference on Integrated Optics, ECIO08, Eindhoven, The Netherlands, 11-13 June 2008.
- [19] Van der Tol, J.J.G.M., Y.S Oei, U. Khalique, R. Notzel and M.K. Smit, "InP-based photonic circuit: comparison of integration techniques", Progress in Quantum Electronics, Volume 34, Issue 4, July 2010, Pages 135-172 .
- [20] Zhang, R. et al: 'Submicron Active-Passive Integration for InP-based Membranes on Silicon', Proc. ECIO 2010, Cambridge (UK), paper ThH1.
- [21] Micallef, J., A. Brincat and W. C. Shiu, "Cation inter-diffusion in GaInP/GaAs single quantum wells", Proceeding of Material. Resource Society. Symposium. Vol. 484, 1998.